International Journal of Microwave and Wireless Technologies, 2014, 6(3/4), 353–360.
doi:10.1017/S1759078714000208

RESEARCH PAPER

Dynamic interference suppression for chipless wireless sensors based on an out-of-band channel estimation method

BERND KUBINA, CHRISTIAN MANDEL, MARTIN SCHÜßLER AND ROLF JAKOBY

A channel estimation method for chipless wireless sensors is presented. The method is developed to suppress interference signals in radio frequency backscatter systems. It uses two adjacent frequency bands to estimate and suppress the disturbing signal of a dynamic interferer. Afterwards a correction of the sensor tag's backscatter signal is achieved. The method has been tested in indoor measurements with a chipless strain sensor and a chipless temperature sensor. A metal block has been deployed as an interferer. In the given scenario, the method has enabled a determination of the sensors' resonance frequencies with relative errors of <2% in average. A general dependence of the estimation robustness on the peak bandwidth is observed.

Keywords: RFID and sensors, Wireless systems and signal processing (SDR, MIMO, UWB, etc.)

Received 15 October 2013; Revised 28 January 2014; first published online 4 March 2014

I. INTRODUCTION

The employment of wireless radio frequency identification (RFID) and wireless sensor systems has grown extensively in the past decade. Nowadays, RFID systems are found in logistics, medical environments, or even supermarkets. Wireless sensors are becoming irreplaceable elements in industrial environments and aid in numerous controls and monitoring tasks.

Motivated by this development, a particular interest arises in the development of chipless wireless RFID and sensing systems. These systems operate in the lower gigahertz range and their tags work entirely in the electromagnetic domain. The wireless tags do not use any semiconductor-based integrated circuits and do not require a local power supply. Hence, they offer application potential in excess of chip-based systems: they can enable operation in the very low-cost regime [1] or in harsh environments, e.g. at very high temperatures.

With a strong similarity to some chipless radio frequency (RF) identification tags [2–4], a promising approach to realize chipless sensor tags is the use of RF backscatter signals with spectral signatures to encode and transmit the measurement value. This principle has been used to realize chipless temperature [5–7], strain [8–10], displacement [11], and gas [12] sensors.

However, one key aspect occurring during the employment of fully chipless RF sensors has been treated very little in the literature, which is the challenge to readout the sensors in time-variant environments. Some static reading scenarios have been presented that face reflections from *standing* objects with reference measurements [3, 4, 8, 9], or time-gating [5, 7, 11]. But the impact of *moving* objects in the vicinity of the reader or the tag has hardly been studied or counteracted [13].

This work presents a channel estimation (CE) method to estimate and suppress the interference caused by a dynamic object in a wireless reading scenario. The interfering signal is characterized in two frequency bands adjacent to the tag's transmission band. Together with an optimization routine, the characterization yields an estimate of the interfering signal and a corrected measurement signal. The proposed method has been successfully tested in two wireless proof-of-concept scenarios with a chipless strain sensor and a chipless temperature sensor. A metallic block acted as a dynamic interferer.

II. OUT-OF-BAND CE METHOD

In a chipless wireless sensor-reading scenario, as drawn in Fig. 1, a reader, the sensor tag, and a number of ambient objects are part of the measurement space. The received signal is a sum of backscatter signals, including interference signals from the objects plus the useful tag response.

For the proposed method, reflections from static objects and the reader antenna mismatch are suppressed by reference measurements. Assuming that an approximate distance between reader and tag antenna is known, time-gating methods filter out background reflections, i.e. reflections from the static or dynamic objects far away from reader and tag. This way, one reduces the number of relevant dynamic interferers to a minimum. In this paper, as a first approach,

Technische Universität Darmstadt, Institute for Microwave Engineering and Photonics, Merckstrasse 25, 64283 Darmstadt, Germany. Phone: +49 6151 1675163
Corresponding author:
B. Kubina
Email: kubina@imp.tu-darmstadt.de

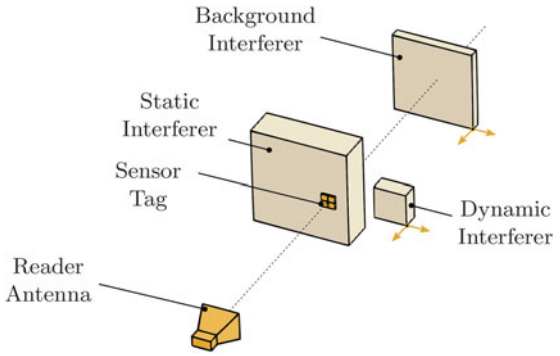

Fig. 1. Wireless sensor scenario: the sensor tag is located close to a static and a dynamic interferer.

one single dynamic interfering object is taken into consideration. A metal block is used as a representative for various moving metallic objects that might be found in an application environment, e.g. a robot arm or a die cutter on a manufacturing site. The block is placed in different positions to imitate a dynamic movement of the interferer.

To analyze this reading scenario the following subsections show a few theoretical considerations as well as a description of the measured signal and its processing to gain an estimate of the dynamic channel impulse response and of the desired tag signal.

A) Theoretical analysis

In a backscatter scenario, the power that is received from an arbitrary object with radar cross section (RCS) is given by the radar equation [14]. According to this, the normalized Rx power from an interfering object in the measurement room is proportional to its cross-section RCS_I. The interferer's normalized Rx signal S_I at the reader can be derived from the radar equation. As a function of the frequency f, it is given by

$$S_I(f) = \sqrt{\mathrm{RCS}_I(f)}\,\frac{A_R f}{\sqrt{4\pi}c_0 r^2}\,e^{j\varphi_I(f)}, \tag{1}$$

with the Rx phase φ_I, the reader-to-object distance r and the speed of light c_0, if an aperture antenna at the reader side with aperture size A_R is assumed.

Setting a metallic block as the interfering object, the block's Rx signal becomes

$$S_M(f) = A_M A_R\,\frac{f^2}{c_0^2 r^2}\,e^{j\varphi_M(f)} \tag{2}$$

with phase φ_M, if the RCS of the block is approximated with $\mathrm{RCS}_M = A_M{}^2 4\pi f^2/c_0{}^2$ and its cross-sectional area is A_M. The signal amplitude of the block backscatter shows a quadratic decrease with increasing distance r and a quadratic increase with increasing frequency f.

According to (1), the desired signal S_T of the sensor tag with RCS_T is

$$S_T(f) = \sqrt{\mathrm{RCS}_T(f)}\,\frac{A_R f}{\sqrt{4\pi}c_0 r^2}\,e^{j\varphi_T(f)} \tag{3}$$

with its Rx phase $\varphi_T(f)$.

The considered group of chipless sensors use the tag's RCS to encode the desired information. The measured value is calculated from a resonance peak in the tag's cross-section RCS_T. Hence, this approach is called frequency position encoding [15].

In the measurement scenario, the useful tag signal S_T adds up with the interfering signal including both amplitudes and phases. The decoding of the measured value from the tag's resonance peak is then strongly affected by this complex sum. The peak can (a) remain a maximum if tag signal and interference signal are in phase, (b) become a minimum for 180° phase shift between the phases of the received signals, i.e. $\varphi_T - \varphi_I = \pi$ or (c) have any amplitude value in between for arbitrary phase constellations. Consequently, one sees the peak position shifting or vanishing in dependence of the local tag and interferer constitution and hence, the measurement decoding becomes erroneous or even impossible.

B) Received signals in practice

Describing the received signal after the above-mentioned reference and time-gating methods, the measured received signal $\overline{S}$ is taken as the sum of the measured tag signal $\overline{S}_T(f)$ and the measured backscatter $\overline{S}_I(f)$ from the dynamic interferer

$$\overline{S}(f) = \overline{S}_T(f) + \overline{S}_I(f). \tag{4}$$

These tag and interference signals, $\overline{S}_T(f)$ and $\overline{S}_I(f)$, can be approximated by the theoretical expressions $S_T(f)$ and $S_I(f)$ in (3) and (1).

The CE method splits up the received signal $\overline{S}(f)$ into three bands: The tag backscatter band B_0 as the set of frequencies between $f_{0,1}$ and $f_{0,2}$, the lower estimation band $B_1 = [f_{1,1}, f_{1,2}]$ and the upper estimation band $B_2 = [f_{2,1}, f_{2,2}]$ as shown in Fig. 2. The tag backscatter band B_0 is the range in which the tag's resonance is expected, and carries both the useful signal and the interfering signal

$$\overline{S}_{B,0}(f) = \overline{S}_T(f) + \overline{S}_I(f) \text{ for} f \in B_0. \tag{5}$$

The presented method assumes that in the two estimation bands the RCS of the tag is negligibly small, so that the measured bands' *Rx* signals $\overline{S}_{B,1}$ and $\overline{S}_{B,2}$ are approximately

$$\overline{S}_{B,1}(f) \approx \overline{S}_I(f), \quad \text{for} f \in B_1, \tag{6}$$

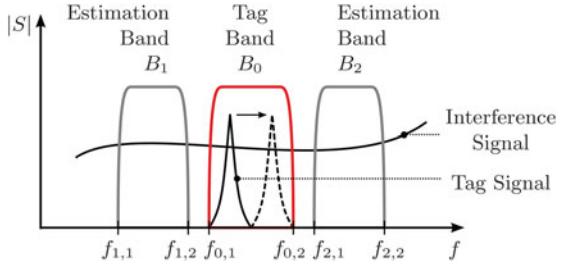

Fig. 2. Principle of the channel estimation method. The tag signal shows a resonance peak, who is tuned by the measurement value. This tag signal is disturbed by the interference signal. The interference signal is characterized in the two estimation bands adjacent to the tag backscatter band.

https://doi.org/10.1017/S1759078714000208 Published online by Cambridge University Press

and

$$\overline{S}_{B,2}(f) \approx \overline{S}_I(f), \text{ for } f \in B_2. \quad (7)$$

Consequently, the two estimation bands allow a view onto the spectral characteristic of the dynamic interferer in a limited frequency range. This separation of the interference signal is a key element of the presented approach. The estimation bands are used to find spectral properties of the interference signal. The spectrum of the interference signal in the central tag backscatter band is afterwards estimated from these properties.

C) Estimation signals

Based on the measured estimation band signals $\overline{S}_{B,1}$ and $\overline{S}_{B,2}$, the CE method aims at finding an estimate $\hat{S}_I$ of the interference signal $\overline{S}_I$ for the central tag backscatter frequency range. This estimate is complex in order to include both magnitude and phase of the interference.

Using the approximations of (6) and (7), the estimation signal $\hat{S}_I$ is settled to approximate amplitude and phase of the lower and upper estimation band signals. So, the two estimation band errors ϵ_1 and ϵ_2

$$\epsilon_1 = \int_{f_{1,1}}^{f_{1,2}} \left|\overline{S}_{B,1}(f) - \hat{S}_I(f)\right| df, \quad (8)$$

$$\epsilon_2 = \int_{f_{2,1}}^{f_{2,2}} \left|\overline{S}_{B,2}(f) - \hat{S}_I(f)\right| df \quad (9)$$

are defined to describe the magnitude of the complex difference between estimate and measured signal in the two estimation bands. The sum error ϵ_t of these two errors

$$\epsilon_t = \epsilon_1 + \epsilon_2 \to 0 \quad (10)$$

is then taken as an optimization/minimization criterion to find a suitable interference signal estimate.

The estimate $\hat{S}_I$ of the unknown interference signal $\overline{S}_I$, is set up as a number of N weighted Dirac pulses

$$\hat{s}_I(t) = \sum_{i=1}^{N} \left(A_i\, e^{j\varphi_i}\, \delta(t-\tau_i) * g_i(t)\right), \quad (11)$$

which are represented in frequency domain by a sum of complex oscillations

$$\hat{S}_I(f) = \sum_{i=1}^{N} A_i e^{j(2\pi f \tau_i - \varphi_i)} G_i(f) \quad (12)$$

with the Fourier-transformed weighting function $G_i(f) = \mathcal{F}(g_i(t))$. As indicated in (2), the RCS of many metallic objects shows a frequency dependent amplitude increase. This behavior is imitated by the weighting function $G_i(f)$

$$G_i(f) = (f - f_o)\alpha_i + 1 \quad (13)$$

with the linear slope α_i and the reference frequency f_o.

This CE approach leads to four unknowns for the ith Dirac pulse: magnitude A_i, phase φ_i, instant of time τ_i, and slope α_i. For a set of N pulses the total number of unknowns becomes then $4N$. These unknowns have to be found with a suitable optimization method to satisfy the criterion of (10). In this work, a sequential optimization algorithm is used, which is described in the following Section D).

After the optimization, the desired tag signal S_T is estimated as $\hat{S}_T$ by subtracting the interference signal estimate $\hat{S}_I$ from the measured Rx signal

$$\hat{S}_T(f) = \overline{S}(f) - \hat{S}_I(f). \quad (14)$$

The tag's resonance peak at f_r, from which the measured value is concluded in a sensor application, is estimated as the frequency $\hat{f}_r$, which shows the largest magnitude in $\hat{S}_T(f)$ within the backscatter band B_o. The difference

$$\begin{aligned}\epsilon_{f_r} &= f_r - \hat{f}_r \\ &= f(\max|\overline{S}_T(f)|) - f(\max|\hat{S}_T(f)|) \quad \text{for} f \in B_o \end{aligned} \quad (15)$$

between the true and estimated resonance frequency as well as the phase estimation error

$$\epsilon_\varphi = \overline{\varphi} - \hat{\varphi} = \angle\overline{S}(f) - \angle\hat{S}_I(f) \quad (16)$$

are taken as measures for the quality of the interference estimation and shown in Section IV for a practical scenario.

D) Sequential optimizer

As described above, the presented CE method assumes a number of N-weighted Dirac pulses to estimate and suppress the unwanted interference signal. In order to find an optimal estimate, $4N$ unknowns have to be found as (12) indicates: the magnitude A_i, phase φ_i, time instant τ_i, and slope α_i of each of the N pulses.

To find the set of variables a sequential optimizer is used, which runs N-sequence steps, and determines magnitude, phase, time instant, and slope of the ith pulse of (11) in one sequence step. This sequential approach is mainly taken to minimize the computational complexity of the optimization problem by avoiding the necessity to optimize a joint $4N$-dimensional criterion.

In the ith sequential step, an initial estimate of the four unknowns is found by using the discrete Fourier transform (DFT) of the estimation bands' received signals $\overline{S}_{B,1}$ and $\overline{S}_{B,2}$. This initial estimate is optimized with the criterion in (10) using (12) with $N = 1$. This optimization leads to an intermediate estimation signal. The intermediate estimation signal is subtracted from the measured signal and the sequence is restarted for $(i+1)$. The final estimate $\hat{S}_P$ is summed up as given in (12) with the set of all optimized variables from all optimization sequences.

III. THE SENSOR TAGS

The presented CE method has been tested with two different chipless sensor tags. This section describes the setup and functionality of the two tags.

https://doi.org/10.1017/S1759078714000208 Published online by Cambridge University Press

The first tag is a strain sensor and has been presented in [8]. The strain sensor is built up as a composite right-/left-handed microstrip mushroom structure. The gap between the two mushroom elements forms a capacity, which is varied by the gap width (see Fig. 3(a)). Together with the line and via inductance a shorted resonant antenna structure is formed. The antenna's resonance can be measured wirelessly as a peak in the RCS. The peak shifts between 3.05 and 3.2 GHz for gap widths between 250 and 600 μm. This behavior can be used to measure corresponding mechanical strains of up to 140%. A photo of the 1.5 × 1.5 cm² large tag is shown in Fig. 3(b).

The second tag is a temperature sensor that has been presented in [16]. The sensor is built from a half-split cylindrical dielectric resonator (DR) placed on a metallic ground plane. An incident RF wave excites the $TE_{011+\delta}$-mode (see Fig. 3(c)) inside the DR, which is seen as a resonance peak in the RCS. The resonance frequency f_r and hence, the peak position, shift temperature-dependent due to the dependency of the DR's permittivity on the temperature ϑ. The sensor's resonance lies at 2.91 GHz at room temperature and shows a sensitivity of $\Delta f_r/\Delta\vartheta = 307$ kHz/K. The resonator has a diameter of 2 cm and height of 1.5 cm, whereas the aluminum ground sheet has a size of 9 cm × 9 cm. A photograph of the tag is shown in Fig. 3(d).

The two tags use very similar principles for the chipless sensing, which is mainly the usage of resonant structures and a detuning of their resonance frequency. They both use frequency-position encoding [15] of the measurement value. While the resonance frequencies of both tags lie about 3 GHz, one main difference between them are their resonance bandwidths. While the strain sensor shows resonance quality factors about 50, the temperature sensor's quality factor is about a factor 11 times higher at 550. The impact of this difference on the performance of the CE method is described in the following Section IV.

IV. MEASUREMENTS

In order to prove the presented interference suppression method and to evaluate its performance, wireless measurements have been performed. During these measurements, a chipless wireless strain sensor tag and a temperature sensor tag have been used. The setup and functionalities of these two tags have been presented in the previous Section III. During the measurements a metallic block acts as an interfering object. The block is placed at different positions to imitate a dynamic movement of the interferer. This imitation assumes a movement of the interferer, which is slow compared to a measurement cycle. Furthermore, the imitation assumes that Doppler shifts due to the movement can be neglected. This negligence appears reasonable, since an object velocity of up to 100 km/h would cause shifts of less than 280 Hz at the operation frequency. This shift would be very small compared to the estimation error margin, which is in the MHz range as presented below.

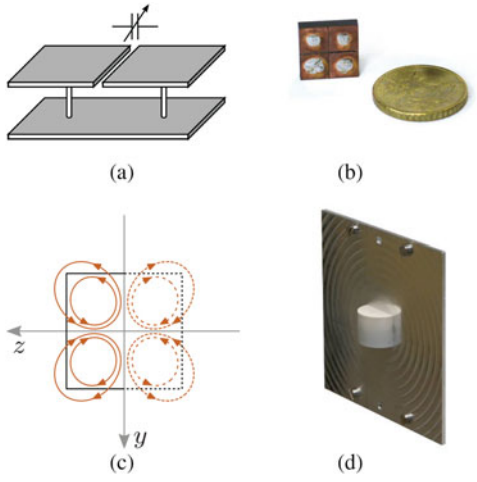

Fig. 3. Photographs of the strain (b) and temperature (d) sensors as well as functionality principles of the sensor tags. (a) The resonant frequency of the strain sensor is detuned by the capacity between the mushroom elements. (c) The $TE_{011+\delta}$ mode used in the temperature sensor.

A) Measurement setup

The measurements have been conducted in a hall where a vector network analyzer, connected to a horn antenna, has been used as a reader. The two sensor tags have been placed in two similar setups on a stand in front of the horn antenna. The setups are shown in Fig. 4(a) for the strain sensor and in 4(b) for the temperature sensor. In both cases, a metallic block has acted as the dynamic interfering object. For the temperature sensor setup, a heat gun and an infra-red camera have been used to control the temperature of the tag.

In the strain sensor setup, the distance d_1 between the tag and horn antenna has been 60 cm. The metal block, which acts as a dynamic interferer, has a cross-section of 4.5 × 9 cm² (18 times the area of the tag). It has been placed in a distance $d_2 = 10$ cm next to the tag as shown in Fig. 5.

For the temperature sensor tag, the distance d_1 between tag and horn antenna has been 85 cm. A metal block with a

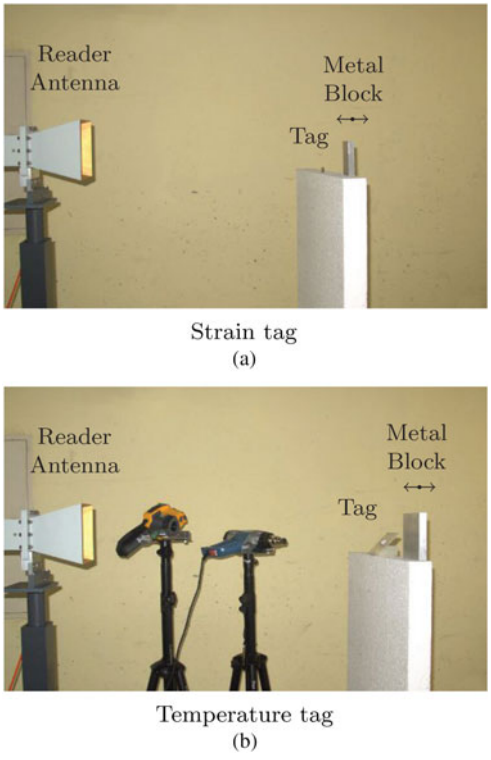

Fig. 4. Photographs of the two measurement setups.

https://doi.org/10.1017/S1759078714000208 Published online by Cambridge University Press

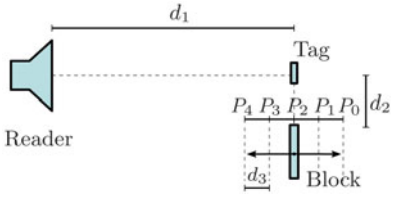

Fig. 5. Top view of the placement of reader antenna, sensor tag, and metal block during the measurements. The block has been placed at five different positions to imitate a dynamic movement of the interferer.

cross-sectional area of 10 × 12 cm² (40 times the area of the DR) has been chosen and placed at $d_2 = 10$ cm next to the tag. In comparison to the strain sensor, the temperature tag shows a higher received power for identical reading distances. Owing to this reason a larger distance d_2 has been chosen to have similar peak powers in both setups. A larger metal block was chosen, to keep the ratio between tag and interference power, i.e. the signal-to-inference ratio (SIR) comparable.

In both setups, the metal block has been placed at five different positions in order to imitate a dynamic movement of the interferer. The five different positions are named P_0 to P_4 and are spaced by $d_3 = 1$ cm as shown in Fig. 5. This positioning includes a shift of the interferer's phase φ_I by 360° at the center-operating frequency of 3 GHz in order to comprise constructive, destructive and intermediate superposition of tag and interference signal. These five block positions have been combined with two different measurement values/resonance frequencies of each tag, so that ten combinations of block position and measurement value are evaluated for each setup.

The measurement values of the strain setup are the gap widths $W_1 = 345$ μm and $W_2 = 535$ μm with resonant frequencies 3.100 and 3.176 GHz. For the temperature tag, ambient temperatures of 20 and 35°C have been set with resonant frequencies at 2.914 GHz and 5.75 MHz higher at 2.920 GHz.

The resonance shift in absolute terms of the temperature tag is about a factor 13 times smaller than for the strain tag. This setting has been chosen intentionally, in order to attain comparable results. As mentioned in Section III, the temperature sensor shows an 11 times higher resonance Q-factor than the strain tag and has an 11 times smaller bandwidth. Hence, the resonance shift of the two setups is nearly identical in relation to the peak bandwidth.

According to the CE approach described in Section II, the subsequently presented measured signals are obtained under assistance of a differential measurement of the 'empty' hall, i.e. without tag and metal block, to minimize the impact of static interferers. Furthermore, time gating has been applied to filter out background interferers.

B) Results

Figure 6 shows the measured signal of the two sensor tags and of the metal blocks separately. For the strain sensor, the resonant peaks at 3.100 and 3.178 GHz are identified in Fig. 6(a). The metal block alone shows a rippled response signal with quadratically increasing amplitude. A comparison between the block response at the two positions P_1 and P_2 shows comparable amplitude but different phase. The ratio between tag peak power and average block interference power is SIR = 0.52.

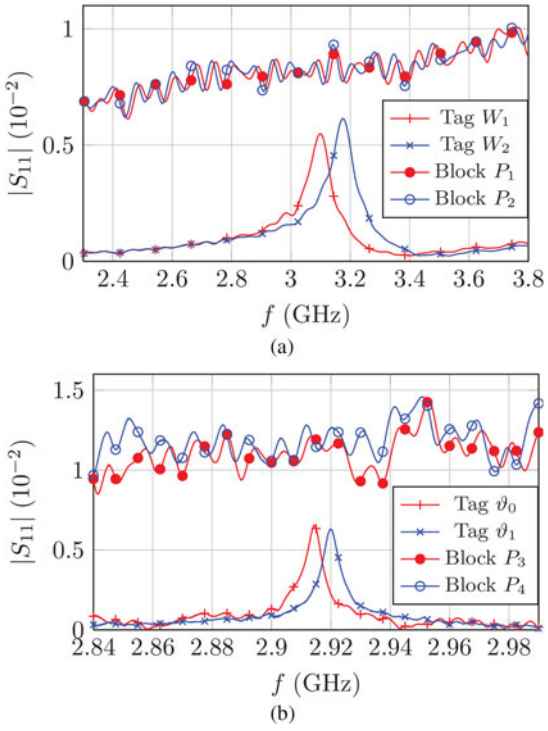

Fig. 6. Measurements of the sensor tags and of the metal block 'alone' in the setup. (a) Strain tag with gap widths W_1 and W_2 and metal block at positions P_1 and P_2. (b) Temperature tag at temperatures θ_1 and θ_2, and the metal block at positions P_3 and P_4.

The resonance peaks of the temperature sensor are seen in Fig. 6(b) with amplitudes of about 6.4×10^{-3}. The backscatter signals of the metallic block are slightly stronger and show stronger ripples than in the strain sensor setup. The SIR in the second setup is 0.3.

Examples of the performance of the CE methods are shown in Fig. 7. When both, tag and block are placed in front of the reader antenna, the received signal does not show the tag peaks any more. A detection of the resonant peak of the tag is not possible in these disturbed Rx cases. The strong distortions are visible in both cases for the strain sensor with block position P_2 and gap width W_1 (see Fig. 7(a)) as well as for the temperature sensor tag with block position P_4 and temperature ϑ_0 (see Fig. 7(b)).

With the presented CE algorithm, estimates of the interference signals are obtained and the difference between Rx signal and interference estimation signals are shown, which yield the tag signal estimates. The tag signal estimates show good reconstructions of the tags' transmission characteristics. Some amplitude differences are visible between the true and estimated peak, which are partly caused by the influence of the metal block onto the radiation pattern of the tags. The decisive peak positions are found with very slight offsets. For the strain sensor example, the difference between the true and estimated peak frequency ϵ_{f_r} (compare (15)) is equal to 2 MHz. For this example, a number of $N = 2$ Dirac pulses was taken to approximate the interference signal with the estimation bands $B_1 = [2.5, 2.8\ \text{GHz}]$ and $B_2 = [3.3, 3.6\ \text{GHz}]$.

For the temperature sensor, the estimation error in the example is $\epsilon_{f_r} = -0.25$ MHz. $N = 1$ Dirac pulse was taken as an approximation with the bands $B_1 = [2.86, 2.89\ \text{GHz}]$ and $B_2 = [2.94, 2.97\ \text{GHz}]$.

https://doi.org/10.1017/S1759078714000208 Published online by Cambridge University Press

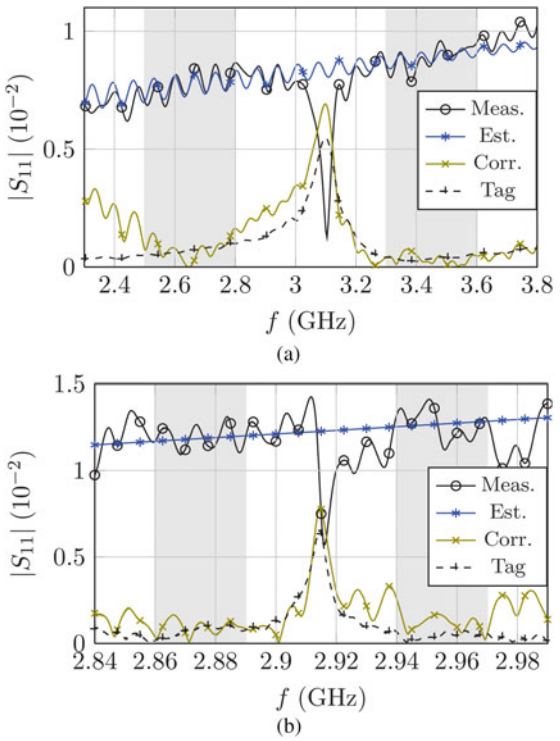

Fig. 7. Exemplary results of the presented CE method: measured (Meas.), estimated (Est.), and corrected (Corr.) signals and the tag-only (Tag) measurement. The two estimation bands are marked grey shaded. (a) For the strain tag with gap $W_1 = 345$ µm and block position P_2, (b) for the temperature tag with $\theta_1 = 20^\circ$ C and block position P_4.

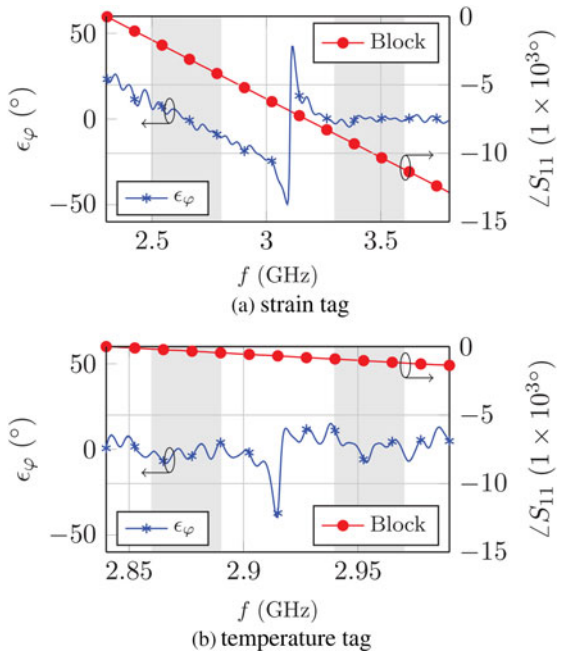

Fig. 8. Phase estimation error ϵ_φ from (16) for the scenarios of Fig. 7 and the absolute phase of the interference signal (Block).

In both setups, the number of Dirac pulses has been chosen as small as possible (to keep the computational effort low) while achieving smallest estimation errors. Higher pulse numbers N did not lead to significantly better results.

Figure 8 shows the phase estimation error ϵ_φ of (16) and the absolute phase of the metal block. Within the estimation bands B_1 and B_2 the phase error lies between $\pm 20^\circ$ and shows largest slope at the estimated resonance positions. A comparison between Figs 8(a) and 8(b) shows the significantly smaller absolute phase steepness of the interference signal, due to the ten times smaller bandwidth of the temperature sensor setup.

With the above-mentioned estimator settings all ten combinations between the two tag resonance positions and the five block positions have been evaluated, leading to the results listed in Fig. 9. For the strain tag, the resonance peak of the tag has been found under support of the CE method with maximum deviations ϵ_{f_r} of -12 to 6 MHz. In comparison, if no CE algorithm is applied, the backscatter band maxima are spread with a maximum error between -102 and 90 MHz.

For the temperature tag, the resonance estimation error ϵ_{f_r} is found within an interval of -0.75 and 0.25 MHz. This result is seen in comparison to peak deviations between -15.50 and 8.00 MHz without the CE method.

C) Result discussion

The results of the measurements show a significant error reduction achieved by the proposed CE method. The impact of the dynamic interferer is strongly reduced.

For the strain sensor tag, an average estimation error of 3.8 MHz is observed, which is equivalent to a relative error of 1.9% in relation to a 200 MHz measurement range. For the temperature sensor, the average estimation error is 0.35 MHz, equivalent to 1.75% relative to a 20-MHz measurement range.

Despite a smaller SIR of the temperature tag measurements, a ten times smaller estimation error in absolute terms is seen compared to the strain sensor setup. A strong correlation with the about ten times higher resonance Q of the temperature sensor is observed. Consequently, one concludes that the estimation error scales with the RCS peak bandwidth of the tag. A higher resonance Q leads to a more robust detection.

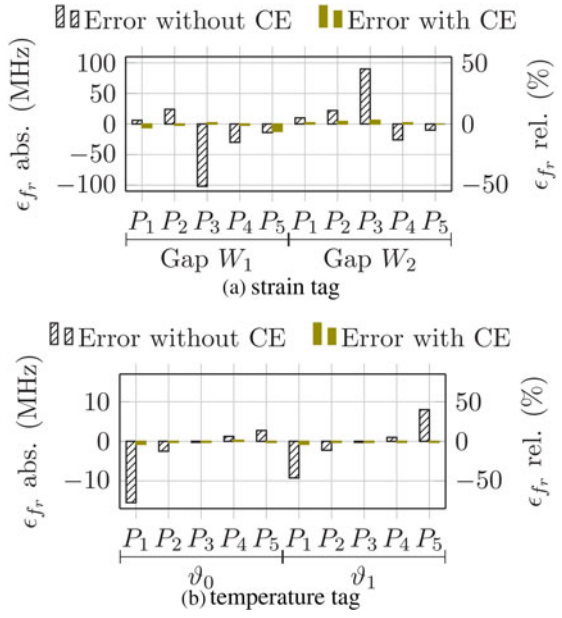

Fig. 9. Resonance position error from (15) for the different tag to block constellations, given in absolute terms and relative to the sensors' frequency ranges.

https://doi.org/10.1017/S1759078714000208 Published online by Cambridge University Press

Furthermore, it should be noted, that the temperature control during the temperature tag setup has been limited in accuracy. From the observations an absolute control inaccuracy of $\pm 0.4^{\circ}$C has to be assumed, which correlates to a resonance offset of ± 0.12 MHZ. Consequently, the average estimation error of 0.35 MHz of the setup is only about three times larger than the temperature uncertainty.

The given estimation results have been achieved with calculations on a standard office computer. Each estimation procedure took about 0.6 s computation time, which consequently allows for real-time applications with update rates in the lower Hertz range. However, a couple of computational speed optimizations are thinkable to improve the estimation speed.

V. CONCLUSION AND OUTLOOK

A channel estimation method for chipless wireless sensor tags has been presented. This method estimates a dynamic interfering signal and corrects the disturbed received signal to regain the spectral signature of the tag.

The method uses two adjacent bands in which the useful tag signal tends to zero to find an estimation signal, which is constructed as a sum of weighted Dirac pulses. A sequential optimizer is used within the method to calculate the estimate on the basis of a DFT signal analysis.

The method has been applied in two indoor reading scenarios with a chipless strain sensor and a chipless temperature sensor. In these scenarios, the interfering signal originated from a metal block placed in different positions to imitate a dynamic movement of an interfering object. Here, the method has proven to be able to successfully suppress the dynamic interferer and to enable a reconstruction of the spectral tag signatures.

During the strain sensor setup with an SIR of 0.52, the reconstruction showed a resonance peak deviation error below 12 MHz and an average deviation of 3.8 MHz equivalent to about 1.9% of the operating frequency range and compared to a deviation of up to 102 MHz without the CE method.

The temperature sensor setup showed a more robust detection, due to its smaller peak bandwidth. With an SIR of 0.30, a reconstruction with an error below 0.75 MHz with an average value of 0.35 MHz has been achieved. This average error relates to about 1.75% of the operating frequency range. Without application of the CE method peak deviations of up to 15.5 MHz have been observed.

The method is seen as one step to bring chipless sensors into dynamic application environments. A general scaling of the estimation error with the peak and estimation bandwidth has been concluded.

Further developments of the method will include a refinement of the optimizer. Furthermore, an application of the method with cross-polarized tags and with chipless RFID tags is planned.

ACKNOWLEDGEMENTS

The authors would like to thank Mr. Andreas Semrad and Mr. Peter Kiesslich for their technical support as well as the German Research Foundation DFG for the support within project JA921/38-1.

REFERENCES

[1] Preradovic, S.; Karmakar, N.C.: Chipless RFID: bar code of the future. IEEE Microw. Mag., **11** (2010), 87–97.

[2] Schüßler, M.; Maasch, M.; Damm, C.; Jakoby, R.: Compact microstrip patch antennas for passive RFID backscatter tags, in 39th Eur. Microwave Conf., Rome, October 2009.

[3] Preradovic, S.; Karmakar, N.C.: Design of fully printable planar chipless RFID transponder with 35-bit data capacity, in 39th Eur. Microwave Conf., Rome, October 2009.

[4] Vena, A.; Perret, E.; Tedjini, S.: Chipless RFID tag using hybrid coding technique. IEEE Trans. Microw. Theory Tech., **59** (12) (2011), 3356–3364.

[5] Cheng, H.; Ebadi, S.; Gong, X.: A low-profile wireless passive temperature sensor using resonator/antenna integration up to 1000°C. IEEE Antennas Wireless Propag. Lett., **11** (2012), 369–372.

[6] Thai, T.T. et al.: A novel passive wireless ultrasensitive RF temperature transducer for remote sensing, in IEEE MTT-S Int. Microwave Symp. Digest, May 2010.

[7] Kubina, B.; Mandel, C.; Schüßler, M.; Sazegar, M.; Jakoby, R.: A wireless chipless temperature sensor utilizing an orthogonal polarized backscatter scheme, in 42nd Eur. Microwave Conf., Amsterdam, October 2012.

[8] Mandel, C.; Schüßler, M.; Jakoby, R.: A wireless passive strain sensor, in IEEE Sensors Conf., Limerick, October 2011.

[9] Melik, R. et al.: Nested metamaterials for wireless strain sensing. IEEE J. Sel. Top. Quantum Electron., **16** (2) 2010, 450–458.

[10] Thai, T.T.; Aubert, H.; Pons, P.; Plana, R.; Tentzeris, M.; DeJean, G.R.: A newly developed radio frequency wireless passive highly sensitive strain transducer, in IEEE Sensors Conf., Limerick, October 2011.

[11] Mandel, C.; Kubina, B.; Schüßler, M.; Jakoby, R.: Passive chipless wireless sensor for two-dimensional displacement measurement, in 41st Eur. Microwave Conf., Manchester, October 2011.

[12] Yang, L.; Orecchini, G.; Shaker, G.; Lee, H.-S.; Tentzeris, M.: Battery-free RFID-enabled wireless sensors, in Int. Microwave Symp., Anaheim, May 2010.

[13] Kubina, B.; Mandel, C.; Schüßler, M.; Jakoby, R.: Dynamic interference suppression for chipless wireless sensors: an out-of-band channel estimation approach, in 43rd Eur. Microwave Conf., Nürnberg, October 2013.

[14] Pozar, D.M.: Microwave Engineering, Wiley, New York, 2005.

[15] Mandel, C.; Kubina, B.; Schüßler, M.; Jakoby, R.: Metamaterial-inspired passive chipless radio-frequency identification and wireless sensing. Ann. Telecommun., **68** (2013) 385–399

[16] Kubina, B.; Schüßler, M.; Mandel, C.; Jakoby, R.: Wireless high-temperature sensing with a chipless tag based on a dielectric resonator antenna, in IEEE Sensors Conf., Baltimore, November 2013.

Bernd Kubina received the diploma degree in Electrical Engineering from the Technische Universität (TU) Darmstadt, Germany, in 2010. Since 2011 he is with the Institute for Microwave Engineering and Photonics at the TU Darmstadt as a Research Associate. His research interests include wireless sensors, RFID systems, and ferroelectric materials.

https://doi.org/10.1017/S1759078714000208 Published online by Cambridge University Press

Christian Mandel received the Diploma degree in Electrical Engineering and Information Technology from the Technische Universität Darmstadt in Germany in 2009. He is currently with the Institute for Microwave Engineering and Photonics at the TU Darmstadt and working toward the Ph.D. His research interests include chipless RFID and chipless wireless sensors.

Martin Schüßler received the Dipl.-Ing. and Ph.D. degrees from the Technische Universität Darmstadt, Germany, in 1992 and 1998, respectively. Since then he is a staff member of the Institute for Microwave engineering and Photonics of the Technische Universität Darmstadt. During his career he worked in the fields of III–V semiconductor technology, microwave sensors for industrial applications, RFID, and small antennas. His current research interests include the application of metamaterials for industrial and biomedical sensing.

Rolf Jakoby received the Dipl.-Ing. and Dr.-Ing. degrees in Electrical Engineering from the University of Siegen, Germany, in 1985 and 1990, respectively. In January, 1991, he joined the Research Center of Deutsche Telekom in Darmstadt, Germany. Since April 1997 he has a full professorship at TU Darmstadt, Germany. His interdisciplinary research is focused on RFID, micro- and millimeter wave detectors and sensors for various applications, and in particular on reconfigurable RF passive devices, based on liquid crystal and ferroelectric technologies. Rolf Jakoby is Editor-in-Chief of "FREQUENZ", a member of the Society for Information Technology (ITG) of the VDE and a member of the IEEE societies MTT and AP. He is the organizer of various workshops, member of various TPCs, and has been chairman of the European Microwave Conference 2007 and the German Microwave Conference 2011. In 1997, he received the ITG-Prize for an excellent publication in the IEEE AP Transactions.

https://doi.org/10.1017/S1759078714000208 Published online by Cambridge University Press